Pergamon

0956-7151(95)00079-8

Acta metall. mater. Vol. 43, No. 11, pp. 4075–4082, 1995
Elsevier Science Ltd

0956-7151/95 $9.50 + 0.00

MODELLING OF THE YIELD STRENGTH OF A HEAVILY WIRE DRAWN Cu–20%Nb COMPOSITE BY USE OF A MODIFIED LINEAR RULE OF MIXTURES

U. HANGEN and D. RAABE

Institut für Metallkunde und Metallphysik, RWTH Aachen, Kopernikusstraße 14, 52056 Aachen, Germany

(Received 20 October 1994; in revised form 10 February 1995)

Abstract—The strength of heavily wire drawn Cu–20 mass% Nb *in situ* composites considerably exceeds the predictions of the linear rule of mixtures (ROM). An analytical model for the calculation of the yield strength of Cu–20 mass% Nb wires is suggested. The approach is a modified linear rule of mixtures (MROM). It regards the yield strength of the composite as the sum of the volumetric weighted average of the experimentally observed yield strengths of the individual pure phases and a Hall–Petch type contribution arising from the impact of the Cu–Nb phase boundaries. The latter term is described in terms of dislocation pile-ups in the Cu matrix and dislocation movement and multiplication in the Nb filaments. The crystallographic texture and filament geometry of both phases is incorporated. The predictions of the model are in very good accordance with experimental data.

Zusammenfassung—Die Festigkeit drahtgezogener Cu–20 gew.% Nb *in situ* Verbundwerkstoffe übertrifft die Vorhersagen der linearen Mischungsregel (ROM) bei weitem. Ein analytisches Modell für die Berechnung der Fließgrenze von Cu–20 gew.% Nb Drähten wird vorgeschlagen. Der Ansatz entspricht einer modifizierten linearen Mischungsregel (MROM). Er betrachtet die Fließgrenze des Verbundwerkstoffes als die Summe des volumenanteilig gewichteten Mittelwertes der experimentell beobachteten Fließgrenzen der einzelnen reinen Phasen und einem Hall–Petch Anteil, der aus dem Einfluß der Cu–Nb Phasengrenzen resultiert. Der letztere Beitrag wird über Versetzungsaufstaus in der Cu Matrix und Versetzungsbewegung und -multiplikation in den Nb Filamenten erklärt. Die kristallographische Textur und die Filamentgeometrie beider Phasen wird einbezogen. Die Vorhersagen des Modells sind in sehr guter Übereinstimmung mit experimentellen Daten.

1. INTRODUCTION

Cu and Nb have negligible mutual solubility in the solid state [1, 2]. Fibre reinforced *in situ* processed metal matrix composites (MMCs) can hence be manufactured by large strain wire drawing of a cast ingot. Cu–Nb composites have been under intensive investigation for the past 15 years [3–13] mainly for the following two reasons.

Firstly, the strength of the deformed MMC is much greater than expected from the linear rule of mixtures (ROM) [5, 6, 9–11]. Several models have been proposed to explain the observed strength anomaly. The phase barrier model by Spitzig *et al.* [3, 6] attributes the strength to the difficulty of propagating plastic flow through the f.c.c.–b.c.c. interfaces (f.c.c. = face-centered cubic, b.c.c. = body-centered cubic). Funkenbusch and Courtney [11] interpret the strength in terms of geometrically necessary dislocations owing to the incompatibility of plastic deformation of the f.c.c. and b.c.c. phase. Although both models obtain a good description of the strength, their application is limited since they depend on fitting parameters. Raabe and Hangen [14] have suggested a physical model which accounts for the dislocation arrangements at the phase boundaries, for the textures [15–17] and for the morphology [3–9] of both phases. Using this approach the tensile strength of the MMC can be described with a minimum input of fitting parameters.

Secondly, owing to the combination of high strength [3–6, 9–11] and good electrical conductivity [18–20] Cu–Nb alloys are considered as candidate MMCs for producing highly mechanically stressed electrical devices, e.g. long-pulse high-field resistive magnets [13, 21, 22].

Whereas the processing [3–7, 24–26], the microstructure [3–9, 25–28] and the mechanical [3–11, 24–28] and electrical [4, 5, 8, 18–20, 29] properties of Cu–20 mass% Nb have been the subject of thorough studies in the past, an analytical model which describes the increase of strength in terms of dislocation arrangements, texture and microstructure nearly without employment of fitting parameters has not yet been obtained. The current study is hence primarily concerned with the introduction of a new dislocation based model [14] for the description of the yield strength of *in situ* processed MMCs. Although all expressions derived are essentially valid also for other wire drawn *in situ* composites consisting of a f.c.c. and

a b.c.c. phase (e.g. Cu–Ta, Cu–Cr, Cu–Mo, Cu–Fe, Cu–V and Cu–W) the current work concentrates on Cu–20 mass% Nb since most of the experimental data are available for this alloy.

2. STRUCTURE OF THE MODEL AND BASIC ASSUMPTIONS

In the current approach the yield strength of the MMC is described in terms of a modified linear rule of mixtures (MROM). It regards the yield strength of the composite as the sum of the volumetric weighted average of the yield strengths of the individual pure phases (ROM), σ_{ROM}, and a Hall–Petch type contribution attributed to the impact of the Cu–Nb phase boundaries, σ_{MMC} [14]. Whereas σ_{ROM} is directly calculated from experimental data, σ_{MMC} is first derived theoretically and subsequently computed on the basis of microstructural data. Both portions, σ_{ROM} and σ_{MMC}, are linearly decomposed into the contribution of the Cu, σ^{Cu}_{ROM}, σ^{Cu}_{MMC}, and of the Nb phase, σ^{Nb}_{ROM}, σ^{Nb}_{MMC}.

The phase boundaries are impenetrable by dislocations. In order to deduce σ_{MMC} the yield strength observed is essentially attributed to the generation of dislocation pile-ups in the Cu matrix and to the movement or multiplication of dislocations inside the filaments (Fig. 1) [14]. However, some other strengthening mechanisms were also reported in the literature. Whereas Pelton *et al.* [27] and Trybus and Spitzig [30] observed areas in the Nb filaments which were completely void of dislocations, Raabe and Hangen [31] observed structurally less ordered areas, i.e. local amorphization of the Nb filaments. Both contributions are, however, not included in the model. The influence of solute foreign atoms is not taken into account due to the negligible mutual solubility of Cu and Nb.

In the as-cast state the Nb dendrites are randomly oriented [15–17]. With beginning wire deformation the dendrites start to rotate [15–17]. For $\eta > 4$ the composite consists of parallel aligned Nb filaments embedded in the Cu matrix. The present model is valid only for a well aligned and homogenous morphology, i.e. for $\eta > 4$, and uniaxial strain. The approach concentrates on wire drawn Cu–20 mass% Nb.

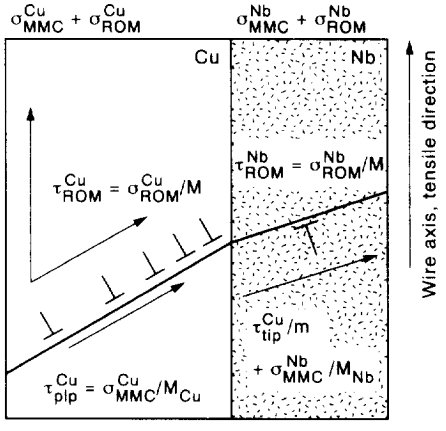

Fig. 1. Schematical presentation of the dislocation arrangements at the phase boundary as incorporated into the model for the calculation of σ_{MMC}.

3. MODIFIED LINEAR RULE OF MIXTURES

The modified linear rule of mixtures (MROM) describes the yield strength of the composite, $\sigma_{RP0.2}$, as the sum of the conventional rule of mixtures, σ_{ROM}, and an additive contribution, σ_{MMC}, arising from the Hall–Petch type interaction between the dislocations and the phase boundaries.

$$\sigma_{RP0.2} = \sigma_{ROM} + \sigma_{MMC}. \tag{1}$$

Both portions, σ_{ROM} and σ_{MMC}, were computed as volumetric weighted average of the strength contributions of the individual phases

$$\sigma_{ROM} = \sigma^{Cu}_{ROM} V_{Cu} + \sigma^{Nb}_{ROM} V_{Nb} \tag{2}$$

$$\sigma_{MMC} = \sigma^{Cu}_{MMC} V_{Cu} + \sigma^{Nb}_{MMC} V_{Nb} \tag{3}$$

where V_{Cu} and V_{Nb} are the volume fractions of Cu and Nb, σ^{Cu}_{ROM} and σ^{Nb}_{ROM} the contributions of the Cu and Nb phases to the ROM, and σ^{Cu}_{MMC} and σ^{Nb}_{MMC} the corresponding contributions resulting from the presence of the phase boundaries.

Since no reliable experimental yield strengths were available for heavily deformed pure Cu (σ^{Cu}_{ROM}) and Nb wires (σ^{Nb}_{ROM}) the linear ROM was calculated from the corresponding ultimate tensile strengths (UTS) [6]. This approximation is admissible in case of large strains ($\eta > 4$) but not in case of low strains ($\eta < 4$), where the UTS exceeds the yield strength by ~20–30%. The true strain of the MMC is defined as $\eta_{MMC} = \ln(A^0/A_{MMC})$ where A^0 and A_{MMC} are the initial and the actual cross-section after deformation. The true strains of Nb and Cu are denoted by $\eta_{Nb} = \ln(t^0/t)$ and $\eta^{Cu} = \ln(\lambda^0/\lambda)$, where t is the thickness and λ the interfilament spacing. From experimental data the ratio of the UTS of pure Nb wires related to that of pure Cu wires is derived as a function of strain

$$R(\eta) \equiv \frac{\sigma^{Nb}_{UTS}(\eta)}{\sigma^{Cu}_{UTS}(\eta)} = \frac{\sigma^{Nb}_{ROM}(\eta)}{\sigma^{Cu}_{ROM}(\eta)}. \tag{4a}$$

It is stipulated that R also holds for the relation σ^{Nb}_{MMC} and σ^{Cu}_{MMC}

$$R(\eta) \equiv \frac{\sigma^{Nb}_{ROM}(\eta)}{\sigma^{Cu}_{ROM}(\eta)} = \frac{\sigma^{Nb}_{MMC}(\eta)}{\sigma^{Cu}_{MMC}(\eta)}. \tag{4b}$$

Following Sevillano [32] the critical stress for dislocation movement between two impenetrable walls is given by

$$\tau_m = \frac{AGb}{2\pi S} \ln\left(\frac{S}{b}\right); \; A \equiv 1.2 \tag{5}$$

where S is the distance of the phase boundaries, G the shear modulus, b the Burgers vector and A a constant valid for mixed dislocations. Figure 1 shows the arrangement of dislocations at the phase boundary as

stipulated in the present approach. The critical stress of a dislocation source which is constrained by two parallel impenetrable walls is given by

$$\tau_{FR} = \frac{AGb}{\pi S} \ln\left(\frac{S}{2b}\right); A \equiv 1.2 \quad (6)$$

i.e. it exceeds the stress required for dislocation movement by nearly a factor of two. The yield strength of the MMC is reached when both parallel phases start to deform plastically. It is hence likely that the critical stress for dislocation movement in the Nb-phase which requires a higher stress than in the Cu matrix defines the yield strength of the MMC. It is assumed that prior to massive plastic deformation of the entire sample, in the Cu, matrix dislocations pile up in front of the phase boundaries (Fig. 1), causing an accumulated strain not exceeding 0.2%. At the tips of the pile-ups a shear stress is generated. Due to this contribution the effective shear stress on the slip planes in the Nb filaments is increased. According to the linear approach [equation (3)] and the configuration shown in Fig. 1 the following equation holds

$$\tau_{tip}^{Cu} = \tau_{plp}^{Cu} \quad n_{plp} = \frac{1}{m}\left(\tau_m - \frac{\sigma_{MMC}^{Nb}}{M_{Nb}}\right) \quad (7)$$

where τ_{tip}^{Cu} is the shear stress acting at the tip of the dislocation pile-up, n_{plp} the number of dislocations accumulated in the pile-up, m the misorientation factor between the slip systems of Cu and Nb and M_{Nb} the Taylor factor of the Nb phase. The critical shear stress for dislocation movement in the Nb filament, τ_m, is calculated according to equation (5). The number of dislocations in a double ended pile-up between two interfaces is given by [33]

$$n_{plp} = \frac{\tau_{plp}^{Cu}\lambda^+(1-\nu_{Cu})}{G_{Cu}b_{Cu}} \quad (8)$$

where $\lambda^+ = \lambda/m_{Cu}$ is the filament spacing normalized by the slip geometry, i.e. λ is the distance measured perpendicular to the phase boundary. The Hall–Petch type contribution, σ_{MMC}, and the shear stress on the Nb slip system, τ, are related according to

$$\sigma_{MMC} = M\tau. \quad (9)$$

Combining equations (7) and (8) leads to

$$(\tau_{plp}^{Cu})^2 \frac{\lambda^+(1-\nu_{Cu})}{G_{Cu}b_{Cu}} = \frac{1}{m}\left(\tau_m - \frac{\sigma_{MMC}^{Nb}}{M_{Nb}}\right). \quad (10)$$

Using equation (4b), equation (10) reads

$$\left(\frac{\sigma_{MMC}^{Cu}}{M_{Cu}}\right)^2 \frac{\lambda^+(1-\nu_{Cu})}{G_{Cu}b_{Cu}} = \frac{1}{m}\left(\tau_m - R\frac{\sigma_{MMC}^{Cu}}{M_{Nb}}\right) \quad (11)$$

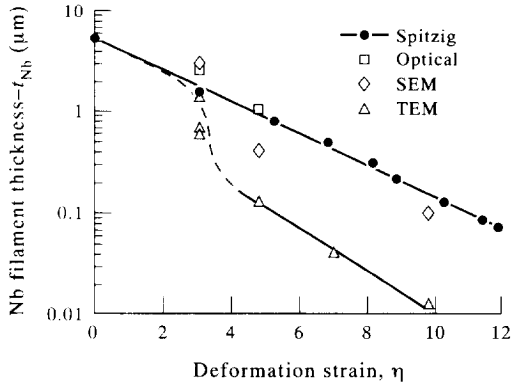

Fig. 2. TEM and SEM data as measured by Verhoeven *et al.* [28]. The data were fitted to be incorporated into the present model (MROM). For low strains ($\eta < 4$) the fitting does not provide correct data [equation (14) and (15)].

after rearrangement one obtains

$$\pm\sigma_{MMC}^{Cu} = -\frac{RM_{Cu}^2 G_{Cu}b_{Cu}}{2\lambda^+(1-\nu_{Cu})M_{Nb}m} \pm \left[\left(\frac{RM_{Cu}^2 G_{Cu}b_{Cu}}{2\lambda^+(1-\nu_{Cu})M_{Nb}m}\right)^2 + \frac{\tau_m M_{Cu}^2 G_{Cu}b_{Cu}}{\lambda^+(1-\nu_{Cu})m}\right]^{1/2}. \quad (12)$$

Since negative stresses are not pertinent in this context the positive sign applies. Using equations (3) and (4) the contribution of the phase boundaries to the yield strength can be written as

$$\sigma_{MMC} = (V_{Cu} + V_{Nb}R)\sigma_{MMC}^{Cu}. \quad (13)$$

4. EXPERIMENTAL INPUT

4.1. Filament geometry

The present model incorporates the filament geometry of wire drawn Cu–20 mass% Nb as measured by Verhoeven *et al.* [28] (Fig. 2). The following expressions for the filament thickness, t, and spacing, λ, were derived by fitting

$$t = t^0 \exp(-\Lambda_{Nb}\eta_{MMC}) \quad (14)$$

$$\lambda = \lambda^0 \exp(-\Lambda_{Cu}\eta_{MMC}). \quad (15)$$

The true strains of both phases related to that of the MMC, Λ_{Cu} and Λ_{Nb}, were calculated as

$$\Lambda_{Cu} = \frac{\eta_{Cu}}{\eta_{MMC}}; \Lambda_{Nb} = \frac{\eta_{Nb}}{\eta_{MMC}}. \quad (16)$$

The ratios were found to be $\Lambda_{Nb} = \Lambda_{Cu} = \Lambda = 0.5$. As starting values $t^0 = 1.2$ μm and $\lambda^0 = 6$ μm were extrapolated from the TEM data [28] (Fig. 2) (TEM = transmisson electron microscope). The initial filament thickness extrapolated deviates from the primary dendrite diameter observed by use of SEM and optical microscopy ($t_{den}^0 = 6.2$ μm) [28] (SEM = scanning electron microscope). As is evident from Fig. 2, the curve fitted from the TEM data is valid only for true strains $\eta > 4$. From equations (14)–(16) where the actual fibre thickness and spacing is

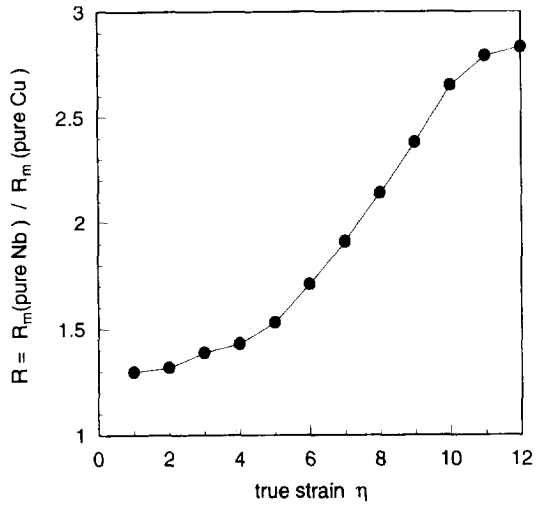

Fig. 3. Ratio of the yield strengths of pure wire drawn Cu and Nb specimens as a function of strain [equation (4)].

expressed in terms of the strain of the composite it becomes apparent that in the present model co-defomation of both phases is stipulated. This behaviour is covered by the results shown in Fig. 2.

4.2. *Linear rule of mixtures*

The model regards the yield strength of the MMC as the sum of the volumetric weighted average of the yield strengths of the individual pure constituents (ROM), σ_{ROM}, and a Hall–Petch type contribution attributed to the presence of internal phase boundaries, σ_{MMC} [14]. Whereas σ_{ROM} is calculated from experimental data, σ_{MMC} is derived theoretically. For the computation of σ_{ROM} data from pure Cu and Nb wires was included. After heavy deformation pure Nb wires reveal a higher UTS, $\sigma_{UTS}^{Cu}(\eta)$, than pure Cu wires, $\sigma_{UTS}^{Cu}(\eta)$. Figure 3 shows the ratio

$$R(\eta) \equiv \frac{\sigma_{UTS}^{Nb}(\eta)}{\sigma_{UTS}^{Cu}(\eta)} = \frac{\sigma_{ROM}^{Nb}(\eta)}{\sigma_{ROM}^{Cu}(\eta)}$$

as function of strain. It is stipulated that this relation also holds for σ_{MMC} [equation (4)].

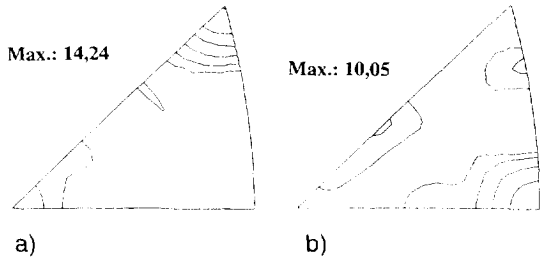

Fig. 4. Texture of the Cu and of the Nb phase in the wire drawn MMC. $\eta = 10$. Measurement by use of X-ray diffraction: (a) Cu, (b) Nb.

4.3. *Crystallographic textures—Taylor factors and slip geometry*

The Cu phase in the MMC reveals a ⟨111⟩ and the Nb phase a ⟨110⟩ fibre texture (Fig. 4). Under "Full Constraints" conditions (FC) [34] the corresponding Taylor factor for Cu amounts to $M_{Cu}^{fc12} = 3.16$ and for Nb to $M_{Nb}^{fc12} = 3.67$ ($\{110\}\langle 111\rangle$ slip systems) or $M_{Nb}^{fc48} = 3.18$ ($\{110\}\langle 111\rangle$, $\{112\}\langle 111\rangle$ and $\{123\}\langle 111\rangle$ slip systems), respectively. In wire drawn Cu–20 mass% Nb the Nb-filaments reveal a curled morphology [35], indicating that FC conditions are not fulfilled locally. Correspondingly, the Taylor factors for "Relaxed Constraints" conditions (RC, relaxation of all shear strains), e.g. [36, 37], have to be additionally considered, i.e. $M_{Nb}^{rc12} = 2.45$ and $M_{Nb}^{rc48} = 2.15$. If single slip is considered the orientation factor for Cu is equal to 0.27 and for Nb equal to 0.4. The misorientation factor between the Cu and the Nb slip systems at the phase boundary then amounts to $m = 0.98$.

5. RESULTS AND DISCUSSION

5.1. *Comparison of simulation and experiment*

Using the experimental input, σ_{MMC} [equation (12)] can be computed as a function of the true strain

$$\sigma_{MMC} = (0.8 + 0.2R) \times \left(- \frac{4.25\ \text{MPa}}{M_{Nb}} R + \left[\left(\frac{4.25\ \text{MPa}}{M_{Nb}} R \right)^2 + 5.9\ \text{MPa}^2 \left(9.25 - \frac{\eta}{2} \right) \right]^{1/2} \right) \exp\left(\frac{\eta}{2} \right). \quad (17)$$

As is evident from Fig. 3, R depends on the degree of deformation. As pointed out previously for Nb, different Taylor factors, M_{Nb}, were considered. The total yield strength of the MMC can then be calculated according to equation (1). In Fig. 5 the yield strengths [6] of the samples, the microstructure of which was studied by Verhoeven *et al.* [28], are depicted together with the simulation results. Since in the original figures of Spitzig *et al.* [6] the UTS is shown, the yield strengths, $\sigma_{RP0.2}$, had to be extracted from the true stress–true strain curves [6]. Four different simulations covering two different variables are shown in Fig. 5.

Firstly, the upper and the lower bound value for the Taylor factor was checked. The largest occurring Taylor factor for Nb was $M_{Nb}^{fc12} = 3.67$ and the smallest one $M_{Nb}^{fc48} = 2.15$. Secondly, dislocation movement [equation (5)] as well as dislocation multiplication [equation (6)] was considered. For low strains ($\eta < 4$) all four predictions show a considerable deviation from the experiments. This is attributed to the fact that the UTS, σ_{UTS}^{Nb}, σ_{UTS}^{Cu}, rather than the yield strengths of the pure wire drawn constituents was used for the computation of σ_{ROM}. Furthermore, in this strain regime the phases are not yet aligned parallel.

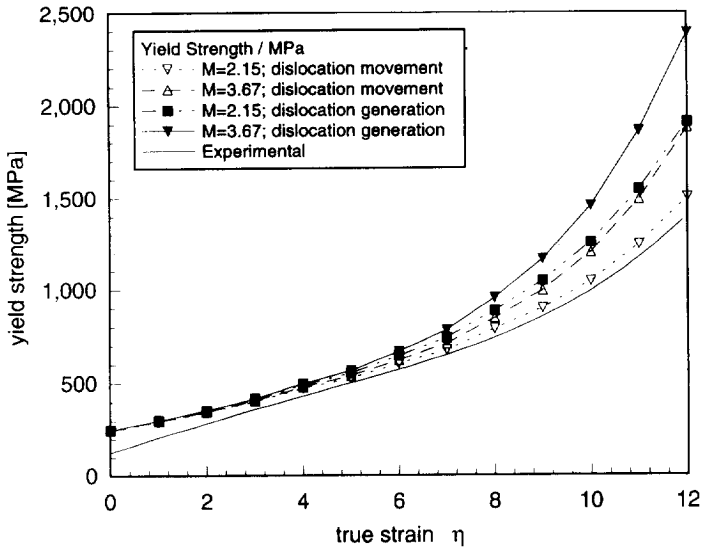

Fig. 5. Predictions of the model compared to experimental results [6]. The simulations were carried out by considering two parameters, viz. the Taylor factor of the Nb phase and the movement or multiplication of dislocations in the filaments, respectively.

The best agreement between the experimental results [6] and the model (Fig. 5) is yielded for the simulation which is based on $M_{Nb}^{fcc48} = 2.15$ and on dislocation movement rather than on multiplication. Both results are physically reasonable. First, the low Taylor factor is attributed to the release of local geometrical constraints, usually imposed by the neighbouring crystals. This assumption is vindicated by the curled morphology of the Nb filaments. Furthermore, it is consistent with Taylor type simulations of crystallographic cold rolling textures of pure polycrystalline Nb which reveal the best agreement with experimental data if the RC approach (relaxation of transverse and longitudinal shear) and 48 potential slip systems are considered [15, 16, 38, 39]. However, the relaxation of strain constraints locally should promote the accumulation of geometrically necessary dislocations [40] in the Nb phase leading to large residual stresses. This effect is consistent with the experimental observations of Bevk *et al.* [4, 5, 18] and Heringhaus *et al.* [17, 19, 20]. Second, since the yield strength rather than the UTS is simulated it seems reasonable that in the first place movement rather than multiplication of dislocations takes place. Furthermore, it was frequently observed that the filament thickness is not homogeneous [8, 14, 19, 20]. It is thus likely that by reaching the yield strength, dislocation multiplication also starts in regions having maximum thickness [equation (6)].

In Fig. 6 both contributions to the total yield strength, i.e. σ_{ROM} and σ_{MMC}, are shown separately. It becomes apparent that the deviation at low strains ($\eta < 4$) is entirely attributed to σ_{ROM}, which was calculated from the UTS rather than from the yield strength of the pure constituents.

5.2. *Checking for physical consistency*

In order to check the physical consistency of the present model, predictions other than the yield strength, viz. the structure of the dislocation pile-ups in the Cu matrix was computed. As a useful measure for a lower bound estimation of the minimum distance, h_{min}, between two parallel pile-ups in front of the phase boundary, the distance which allows for two parallel dislocations to pass each other under an externally imposed stress contribution, σ_{MMC}^{Cu}, was chosen [Fig. 7(a)]

$$h_{min} = \frac{G_{Cu} b_{Cu} M_{Cu}}{2\pi(1 - \nu_{Cu})} \cdot \frac{1}{\sigma_{MMC}^{Cu}}. \tag{18}$$

Considering the number of dislocations per pile-up, n_{plp}

$$n_{plp} = \frac{\sigma_{MMC}^{Cu}}{M_{Cu}} \cdot \frac{\lambda^{+}(1 - \nu_{Cu})}{G_{Cu} b_{Cu}} \tag{19}$$

the dislocation density which is assembled in such configurations, ρ_{dis}, amounts to [Fig. 7(b)]

$$\rho_{dis} = \frac{n_{plp}}{\lambda^{+}/2} \cdot \frac{1}{h} = 2\pi\left(\frac{\sigma_{MMC}^{Cu}(1 - \nu_{Cu})}{G_{Cu} b_{Cu} M_{Cu}}\right)^2. \tag{20}$$

According to this description the maximum dislocation density accumulated in the pile-ups in front of the phase boundaries amounts to $\rho_{dis}(\eta = 12) = 3.3 \times 10^{12}\ m^{-2}$ and the minimum distance between parallel pile-ups to $h_{min}(\eta = 12) = 8$ nm. Albeit the number of additional dislocations, $\rho_{dis}(\eta = 12)$, is quite small and the distance between pile-ups, h_{min}, quite narrow, three features which are regarded as a measure for the physical consistency of the model are elucidated. First, the h_{min} and ρ_{dis} values predicted are within a reasonable order of magnitude [Fig. 7(a,b)].

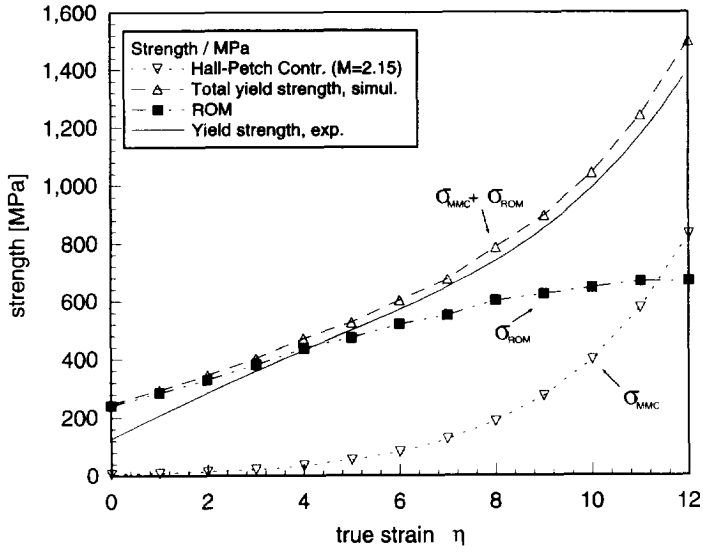

Fig. 6. Results of the simulation ($M_{Nb}^{fit} = 2.15$, dislocation movement) compared to experimental results [6]. Both contributions to the total yield strength, i.e. σ_{ROM} and σ_{MMC}, are shown separately. It becomes apparent that the deviation at low strains ($\eta < 4$) is entirely attributed to σ_{ROM}, which was calculated from the UTS rather than from the yield strength of the pure constituents.

Second, the true strain imposed by such dislocation configurations in the Cu matrix is for all degress of deformation confined to the microplastic regime, i.e. it never exceeds $\eta = 10^{-3}$. Third, the values computed are not in contradiction to TEM experiments [8, 9, 25, 27, 28, 30]. However, there is also not yet any direct evidence for the occurrence of dislocation pile-ups in front of the phase boundaries. This is essentially attributed to two reasons. First, pile-up configurations arranged in such a narrow grid are mechanically not very stable and tend to dissolve during TEM preparation. This is particularly likely if preparation methods like dimpling and ion beam bombardment are employed, e.g. [27, 28, 30]. Second, dynamic recovery and dynamic recrystallization which have been observed by Spitzig and coworkers, e.g. [6, 30], remove pile-up configurations at large strains.

In addition to the investigation of the physical consistency of these internal variables the predictions of the MROM were also successfully used for simulating the yield strengths of Cu-base composites with less then 20% Nb content [41].

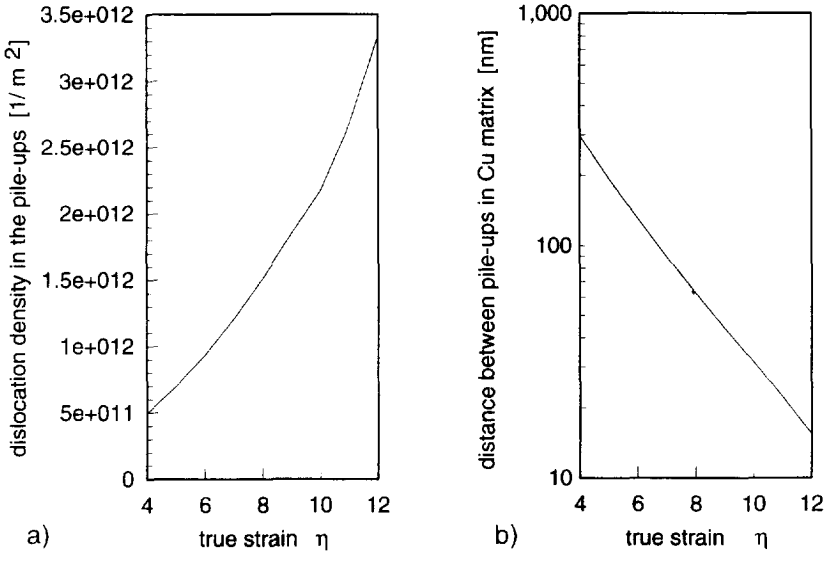

Fig. 7. (a) Lower bound estimation of the minimum distance between parallel pile-ups as a function of strain, $h_{min}(\eta = 12) = 8$ nm. (b) Simulated dislocation density accumulated in the pile-ups in front of the phase boundaries as a function of strain, $\rho_{dis}(\eta = 12) = 3.3 \times 10^{12}\ m^{-2}$.

5.3. Comparison with other models

A comparison of the MROM with the phase barrier model of Spitzig [3, 6] and the model of Funkenbush and Courtney [11] is difficult since in both approaches fitting parameters were employed. The Hall–Petch type simulation of Spitzig [3, 6] and the present MROM approach bear a certain resemblance. Both models attribute the strength to the difficulty of propagating plastic flow through the f.c.c.–b.c.c. interfaces. Whereas the first one [3, 6] is essentially derived by fitting of experimental data, the latter one is based on a physical approach. Since it also leads to a Hall–Petch type relationship, the MROM, in particular the contribution σ_{MMC} can be regarded as a suitable supplementary physical derivation of the barrier model introduced by Spitzig *et al.* [3, 6].

Comparatively, there are less similarities between the MROM and the model of Funkenbush and Courtney [11]. The latter approach is based on a work hardening mechanism, viz. on the generation of geometrically necessary dislocations owing to the incompatibility of plastic deformation of the f.c.c. and b.c.c. phases. This approach is at first sight opposed by the experimental fact that the ratio between the yield and the tensile strength of the MMC is 80% even for heavily wire drawn samples. If the strengthening mechanism was based on such a type of work hardening [11], however, one would for heavily deformed specimens expect a much smaller difference between the yield and the tensile strength. As a possible explanation of this contradiction, the occurrence of dynamic recovery and recrystallization which was observed by Spitzig *et al.* [6, 30] is conceivable.

The model of Sevillano [32] overestimates the yield strength of Cu–Nb when tested with the data of Verhoeven *et al.*, e.g. [28]. The mechanisms proposed as being critical, viz. the movement or multiplication of dislocations in the filaments, however, seem to be relevant and were hence used in the present approach. It might be a flaw in Sevilliano's model [32] that not the local but only the externally imposed load is considered, i.e. dislocation pile-ups in the Cu matrix which increase the shear stress in the Nb filaments [14] are not taken into account explicitly.

6. CONCLUSIONS

A modified linear rule of mixtures (MROM) for the description of the yield strength of a wire drawn Cu–20 mass% Nb composite was suggested. It regards the yield strength of the composite as the sum of the volumetric weighted average of the yield strengths of the individual pure phases and a Hall–Petch type contribution which results from the impact of the Cu–Nb phase boundaries. The latter term is described in terms of dislocation pile-ups in the Cu matrix and the movement or multiplication of dislocations in the Nb filaments. The crystallographic texture and filament geometry of both phases was considered. The predictions reveal a very good agreement with experimental data. It was shown that first, a physical model is able—nearly without use of fitting parameters—to produce a very good description of the experimentally observed yield strength, and second, additional microstructural data such as the structure of pile-up configurations can be predicted.

REFERENCES

1. D. J. Chakrabati and D. E. Laughlin, *Bull. Alloy Phase Diagrams* **2**, 936 (1982).
2. G. I. Terekhov and L. N. Aleksandrova, *Izv. Akad. Nauk SSR. Metally* **4**, 210 (1984).
3. W. A. Spitzig, *Acta metall. mater.* **39**, 1085 (1991).
4. K. R. Karasek and J. Bevk, *J. appl. Phys.* **52**, 1370 (1981).
5. J. Bevk, J. P. Harbison and J. L. Bell, *J. appl. Phys.* **49**, 6031 (1978).
6. W. A. Spitzig, A. R. Pelton and F. C. Laabs, *Acta metall.* **35**, 2427 (1987).
7. F. Heringhaus, D. Raabe, L. Kaul and G. Gottstein, *Metall.* **6**, 558 (1993).
8. F. Heringhaus, D. Raabe and G. Gottstein, *Metall.* **48**, 287 (1994).
9. L. S. Chumbley, H. L. Downing, W. A. Spitzig and J. D. Verhoeven, *Mater. Sci. Engng A* **117**, 59 (1989).
10. T. H. Courtney, in *New Developments and Applications in Composites* (edited by D. Kuhlmann-Wilsdorf and W. C. Harrigan Jr), p. 1. TMS-AIME (1978).
11. P. D. Funkenbusch and T. H. Courtney, *Acta metall.* **33**, 913 (1985).
12. G. Wassermann, *Verbundwerkstoffe*, p. 63. DGM, Oberursel (1981).
13. J. D. Embury, M. A. Hill, W. A. Spitzig and Y. Sakai, *MRS Bull.* **8**, 57 (1993).
14. D. Raabe and U. Hangen, *Proc. 15th Risø Int. Symp.* (edited by S.I. Andersen, J.B. Bilde-Sørensen, T. Lorentzen, O.B. Pedersen and N.J. Sørensen), p. 487. Risø, Denmark (1994).
15. D. Raabe, J. Ball and G. Gottstein, *Scripta metall. mater.* **27**, 211 (1992).
16. D. Raabe and G. Gottstein, *J. Physique IV* **C7**, suppl. *J. Physique III* **3**, 1727 (1993).
17. F. Heringhaus, D. Raabe, U. Hangen and G. Gottstein, Proc. ICOTOM 10, *Mater. Sci. Forum* **157–162**, 709 (1994).
18. F. Habbal and J. Bevk, *J. appl. Phys.* **54**, 6543 (1983).
19. D. Raabe and F. Heringhaus, *Physica status solidi* (a) **142**, 473 (1994).
20. F. Heringhaus, D. Raabe and G. Gottstein, *Acta metall.* **43**, 1467 (1995).
21. F. Herlach, *IEEE Trans. Magnets* **24**, 1049 (1988).
22. H.-J. Schneider-Muntau, *IEEE Trans. Magnets* **18**, 32 (1982).
24. S. Pourrahmi, H. Nayeb-Hashemi and S. Foner, *Metall. Trans.* **23A**, 573 (1991).
25. J. D. Verhoeven, W. A. Spitzig, F. A. Schmidt, P. D. Krotz and E. D. Gibson, *J. Mater. Sci.* **24**, 1015 (1989).
26. P. D. Funkenbusch, T. H. Courtney and D. G. Kubisch, *Scipta metall.* **18**, 1099 (1984).
27. A. R. Pelton, F. C. Laabs, W. A. Spitzig and C. C. Cheng, *Ultramicroscopy* **22**, 251 (1987).
28. J. D. Verhoeven, L. S. Chumbley, F. C. Laabs and W. A. Spitzig, *Acta metall. mater.* **39**, 2825 (1991).
29. H. E. Cline, B. P. Strauss, P. M. Rose and J. Wulff, *J. appl. Phys.* **37**, 5 (1966).
30. C. Trybus and W. A. Spitzig, *Acta metall.* **37**, 1971 (1989).
31. D. Raabe and U. Hangen, *Mater. Lett.* **22**, 155 (1995).
32. J. G. Sevillano, *J. Physique III* **6**, 967 (1990).
33. G. Leibfried, *Z. Physik* **130**, 214 (1951).
34. G. I. Taylor, *J. Inst. Metals* **62**, 307 (1938).

35. W.F. Hosford Jr, *Trans. TMS-AIME* **230,** 12 (1964).
36. H. Honneff and H. Mecking, in *Proc. ICOTOM* 6 (edited by S. Nagashima), p. 347. ISIJ (1981).
37. U. F. Kocks and H. Chandra, *Acta metall.* **30,** 695 (1982).
38. D. Raabe and K. Lücke, *Z. Metallk.* **85,** 302 (1994).
39. D. Raabe and K. Lücke, Proc. ICOTOM 10, *Mater. Sci. Forum* **157–162,** 1469 (1994).
40. M. F. Ashby, *Phil. Mag.* **21,** 399 (1970).
41. D. Raabe and U. Hangen, *Comput. Mater. Sci.* In press.